Matter

CellPress

Article

Designing non-textured, all-solid, slippery hydrophilic surfaces

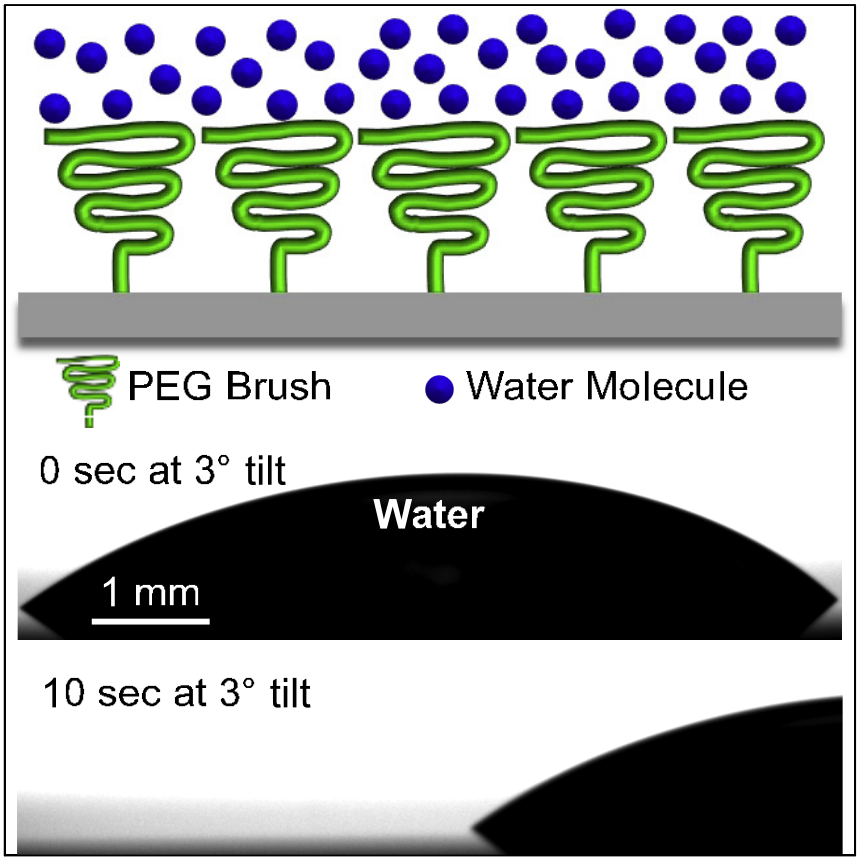

We designed non-textured, all-solid, slippery hydrophilic (SLIC) surfaces by covalently grafting polyethylene glycol brushes to smooth solid substrates above a critical grafting density, which occurs when tethered brush size is equal to inter-tether distance. Our SLIC surfaces demonstrated exceptional performance in condensation and fouling resistance compared with non-slippery hydrophilic and slippery hydrophobic surfaces. We firmly believe that SLIC surfaces constitute an emerging class of surfaces with the potential to benefit multiple technological landscapes ranging from thermofluidics to biofluidics.

Hamed Vahabi, Sravanthi Vallabhuneni, Mohammadhasan Hedayati, ..., Matt J. Kipper, Nenad Miljkovic, Arun K. Kota

akota2@ncsu.edu

Highlights

Elucidated design of non-textured, all-solid, slippery hydrophilic (SLIC) surfaces

SLIC surfaces are ideal for sustained dropwise condensation

SLIC surfaces display outstanding fouling resistance

3 **Understanding**
Dependency and conditional studies on material behavior

Vahabi et al., Matter 5, 1–11
December 7, 2022
https://doi.org/10.1016/j.matt.2022.09.024

Please cite this article in press as: Vahabi et al., Designing non-textured, all-solid, slippery hydrophilic surfaces, Matter (2022), https://doi.org/10.1016/j.matt.2022.09.024

Matter

CellPress

Article

Designing non-textured, all-solid, slippery hydrophilic surfaces

Hamed Vahabi,[1,8] Sravanthi Vallabhuneni,[1,2,8] Mohammadhasan Hedayati,[3] Wei Wang,[1,2,4] Diego Krapf,[5] Matt J. Kipper,[3] Nenad Miljkovic,[6,7] and Arun K. Kota[1,2,9,*]

SUMMARY

Slippery surfaces are sought after because of their wide range of applications in self-cleaning, drag reduction, fouling resistance, enhanced condensation, biomedical implants, etc. Recently, non-textured, all-solid, slippery surfaces have gained significant attention because of their advantages over super-repellent surfaces and lubricant-infused surfaces. Currently, almost all non-textured, all-solid, slippery surfaces are hydrophobic. In this work, we elucidate the systematic design of non-textured, all-solid, slippery hydrophilic (SLIC) surfaces by covalently grafting polyethylene glycol brushes to smooth substrates. Furthermore, we postulate a plateau in slipperiness above a critical grafting density, which occurs when the tethered brush size is equal to the inter-tether distance. Our SLIC surfaces demonstrate exceptional performance in condensation and fouling resistance compared with non-slippery hydrophilic surfaces and slippery hydrophobic surfaces. Based on these results, SLIC surfaces constitute an emerging class of surfaces with the potential to benefit multiple technological landscapes ranging from thermofluidics to biofluidics.

PROGRESS AND POTENTIAL

Water droplets tend to move and slide easily on non-stick coatings. Such slipperiness is intuitive because almost all non-stick coatings have hydrophobic (i.e., water-repellent) surfaces, which do not stick much to water. On the contrary, water spreads and sticks easily to hydrophilic (i.e., water-loving) surfaces. So, hydrophilic surfaces, which allow water droplets to move and slide easily, are counter-intuitive and rare. In this work, we divulge the design principles for making such slippery hydrophilic (SLIC) surfaces. Such SLIC surfaces constitute an emerging class of surfaces with significant potential to benefit multiple technological landscapes ranging from thermofluidics to biofluidics.

INTRODUCTION

Slippery surfaces (i.e., surfaces enabling high mobility of liquids) have received significant attention due to their wide range of applications in self-cleaning, drag reduction, enhanced condensation, biomedical implants, etc.[1–6] In the past 2 decades, most slippery surfaces have been fabricated using two approaches, both of which rely on principles of fluid-film lubrication.[7] The first approach employs super-repellent surfaces,[8–12] which use texture to trap pockets of air at the solid surface. The trapped air acts as a gaseous lubricant, reducing the solid-liquid interfacial area and inducing slip at the liquid-air interface.[13,14] The second approach employs lubricant-infused surfaces,[15,16] which use texture to trap pockets of a liquid, immiscible with the contacting liquids, at the solid surface. The trapped immiscible liquid acts as a liquid lubricant, reducing the solid-liquid interfacial area and inducing slip at the liquid-liquid interface.[17] Despite the appeal of super-repellent surfaces and lubricant-infused surfaces, they lose slipperiness due to damage of texture, depletion of air via dissolution or external pressure, or depletion of lubricant via evaporation or repeated use.[18–22] To circumvent these issues, non-textured, all-solid slippery surfaces have been developed by covalently grafting brushes to substrates (i.e., tethering oligomers or polymers to surfaces).[23,24] Since these surfaces are non-textured and all-solid, concerns related to damage of texture and depletion of fluid are greatly mitigated. Nearly all non-textured, all-solid, slippery surfaces are hydrophobic.[23–27] There are very few reports of non-textured, all-solid, slippery

Please cite this article in press as: Vahabi et al., Designing non-textured, all-solid, slippery hydrophilic surfaces, Matter (2022), https://doi.org/10.1016/j.matt.2022.09.024

hydrophilic surfaces,[28–31] and no studies have systematically investigated or elucidated the design of such surfaces. In this work, we demonstrate that non-textured, all-solid, slippery hydrophilic surfaces can be designed by covalently binding high-surface-energy brushes to smooth substrates, only at sufficiently high grafting densities, resulting in both physical and chemical homogeneity. Furthermore, we postulate a plateau in slipperiness above a critical grafting density, which occurs when the tethered brush size (i.e., twice the Flory radius[32]) is equal to the inter-tether distance. This plateau in slipperiness occurs because, at or above the critical grafting density, water molecules tend to move past the tethered brushes primarily via in-plane motion, with negligible penetration between the brushes, resulting in maximum and constant slipperiness. Building on this understanding, we fabricated slippery hydrophilic (SLIC) surfaces by covalently binding polyethylene glycol (PEG) brushes to smooth substrates with a rapid (<10 min) grafting-to approach. Our SLIC surfaces demonstrate exceptional performance in condensation and fouling resistance compared with conventional (i.e., non-slippery) hydrophilic surfaces and slippery hydrophobic surfaces. Based on these results, non-textured, all-solid, slippery hydrophilic surfaces (e.g., SLIC surfaces) constitute an emerging class of surfaces with the potential to benefit multiple technological landscapes ranging from thermofluidics to biofluidics.

RESULTS AND DISCUSSION

Hydrophilic surfaces can be fabricated by covalently attaching high-surface-energy oligomeric brushes (e.g., PEG brushes) to a solid surface.[33] Such hydrophilic surfaces can display slipperiness when contact angle hysteresis Dq (i.e., the difference between advancing contact angle q_{adv} and receding contact angle q_{rec}) is low. Low-contact-angle hysteresis can be achieved when a surface has low physical and chemical inhomogeneities.[34,35] Non-textured (i.e., smooth) surfaces with very low surface roughness display low physical inhomogeneity. High grafting density s leads to low chemical inhomogeneity. When hydrophilic PEG brushes are grafted to smooth surfaces, slipperiness increases with increasing grafting density. This is because, at lower grafting densities, water molecules tend to penetrate the space between the PEG brushes (see Figure 1A), resulting in pinning and higher hindrance to lateral mobility of water droplets, which in turn leads to lower slipperiness (i.e., higher Dq). As grafting density increases, the penetration of water molecules between the PEG brushes decreases, resulting in lower pinning and lower hindrance to lateral mobility of water droplets, which in turn leads to increasing slipperiness (i.e., decreasing Dq). We postulate that at or above a critical grafting density (i.e., s R s_{crit}), where the brush size (i.e., twice the Flory radius, $2R_F$) is equal to the inter-tether distance, slipperiness is maximum (i.e., Dq is minimum) and constant. This is because, at or above the critical grafting density, water molecules tend to move past the oligomeric brushes primarily via in-plane motion with negligible penetration (see Figure 1B), possibly due to an ice-like hydration layer.[36–38] These physical insights can be conveniently expressed in terms of the non-dimensional slipperiness factor s = s= s_{crit}. When s < 1, it signifies a regime where slipperiness increases with increasing graft-ing density, and when s R 1, it signifies a regime of maximum and constant slipper-iness. So, s > 1 is a prudent criterion for designing non-textured, all-solid, slippery hydrophilic surfaces.

Building on this understanding, in this work, we fabricated SLIC surfaces by covalently grafting PEG brushes (molecular weight, M z 330 Da) to silicon wafers using a rapid grafting-to approach (see Figure 1C). We chose silicon wafers as substrates to minimize physical inhomogeneities (i.e., surface roughness, R_{rms}). We chose PEG

[1]Department of Mechanical Engineering, Colorado State University, Fort Collins, CO 80523, USA

[2]Department of Mechanical and Aerospace Engineering, North Carolina State University, Raleigh, NC 27695, USA

[3]Department of Chemical and Biological Engineering, Colorado State University, Fort Collins, CO 80523, USA

[4]Department of Mechanical, Aerospace and Biomedical Engineering, University of Tennessee, Knoxville, TN 37996, USA

[5]Department of Electrical and Computer Engineering, Colorado State University, Fort Collins, CO 80523, USA

[6]Department of Mechanical Science and Engineering, Department of Electrical and Computer Engineering, Materials Research Laboratory, University of Illinois at Urbana – Champaign, Urbana, IL 61801, USA

[7]International Institute of Carbon Neutral Energy Research (WPI-I2CNER), Kyushu University, 744 Motooka, Fukoka 819-0395, Japan

[8]These authors contributed equally

[9]Lead contact

*Correspondence: akota2@ncsu.edu

https://doi.org/10.1016/j.matt.2022.09.024

Please cite this article in press as: Vahabi et al., Designing non-textured, all-solid, slippery hydrophilic surfaces, Matter (2022), https://doi.org/10.1016/j.matt.2022.09.024

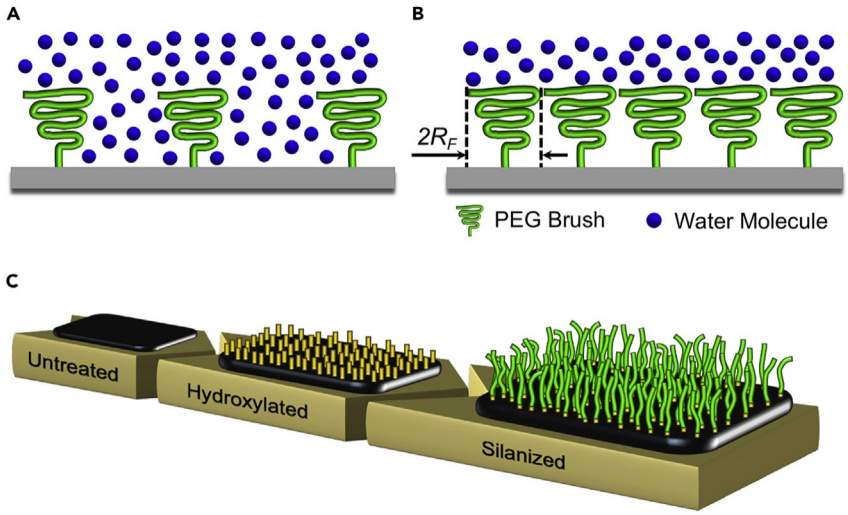

Figure 1. Design and fabrication of SLIC surfaces

(A) Schematic depicting significant penetration of water molecules between PEG brushes at low grafting densities.

(B) Schematic depicting negligible penetration of water molecules between PEG brushes at the critical grafting density.

(C) Schematic depicting the fabrication of SLIC surfaces via hydroxylation and silanization; hydroxyl groups (yellow), PEG brushes (green). Schematics are not to scale and do not depict the precise molecular conformation of PEG brushes.

functional groups to render high solid surface energy, which makes the surfaces hydrophilic. We used a simple and rapid liquid phase silanization[39] (see experimental procedures) to covalently graft PEG brushes (see XPS spectra, Figure 2A) to hydroxylated silicon wafers, while maintaining low surface roughness (R_{rms} < 1 nm; see Figure 2B). To understand the influence of grafting density on wettability and slipperiness, we systematically tuned the non-dimensional slipperiness factor s by tailoring the silanization time t_{sil} (see Note S1 and Table S1). At different t_{sil}, we estimated the grafting density (in chains nm^2), s = ðhrN_A x 10^{21}Þ=M; here, h is the thickness of the PEG layer (in nm) estimated from ellipsometry (see experimental procedures), r is the density of PEG (in g cm^3), N_A is Avogadro's number, and M is the number averaged molecular weight of PEG (in Da). We estimated the critical grafting density s_{crit} = 1=ð2 3 R^2Þ, assuming hexagonal packing with a grafting density s. At t_{sil} = 0 min, water droplets completely spread (static contact angle, q = 0) and did not slide on hydroxylated silicon wafers. As t_{sil} increased, the dynamic contact angles (i.e., q_{adv} and q_{rec}) of water increased (see Figure 2C), indicating increasing covalent grafting of PEG brushes, resulting in increasing s. In addition, as t_{sil} increased, Dq decreased (see Figure 2D), indicating a decrease in inhomogeneities on the sur-face as s / 1. At t_{sil} = 7 min, we estimated that s > 1 for PEG brushes, indicating the onset of maximum and constant slipperiness regime with q_{adv} = 39, q_{rec} = 36, and Dq = 3. For t_{sil} R 7 min, we obtained SLIC surfaces (see Figure 2E and Video S1) with nearly constant contact angles and contact angle hysteresis, confirming that s > 1 signifies a regime of maximum and constant slipperiness. In a similar manner, we also fabricated SLIC surfaces using longer PEG chains (M z 462 Da; see Note S2 and Table S2) at s > 1 reaffirming the criterion for designing non-textured, all-solid, slippery hydrophilic surfaces.

In addition to elucidating the underlying design principles and fabricating SLIC surfaces, we evaluated the performance of our SLIC surfaces in relevant thermofluidic

Please cite this article in press as: Vahabi et al., Designing non-textured, all-solid, slippery hydrophilic surfaces, Matter (2022), https://doi.org/10.1016/j.matt.2022.09.024

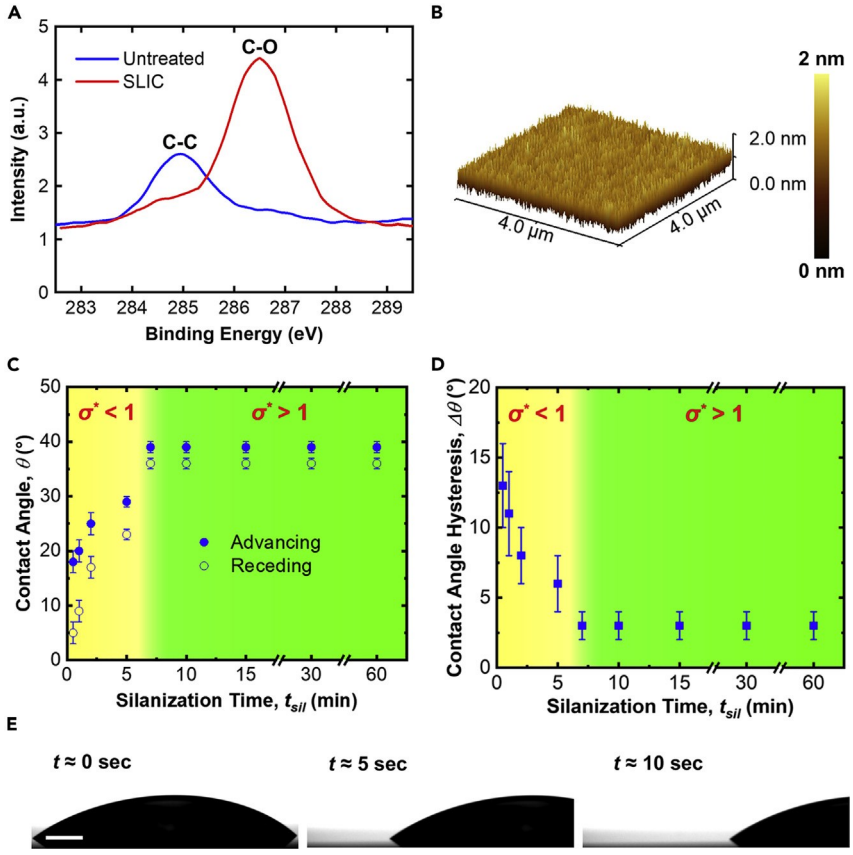

Figure 2. Characterization of SLIC surfaces

(A) High resolution C1s XPS spectra of untreated silicon and SLIC surfaces. The C-C peak (at 285 eV) on untreated silicon is due to the presence of the adventitious carbon. The C-O peak (at 286.5 eV) on SLIC surface indicates the presence of PEG brushes.

(B) AFM image depicting the topography of SLIC surface with surface roughness R_{rms} < 1 nm, indicating low physical inhomogeneity.

(C) Advancing and receding contact angles of water on PEG functionalized surfaces at different silanization times, t_{sil}. Data are represented as mean G standard deviation.

(D) Contact angle hysteresis of water on PEG functionalized surfaces at different silanization times, t_{sil}. Data are represented as mean G standard deviation.

(E) Time-lapse images showing a water droplet (20 mL) sliding easily on a tilted SLIC surface. Scale bar represents 1 mm.

and biofluidic applications. Specifically, our SLIC surfaces are ideal for enhancing condensation heat transfer of aqueous liquids because they simultaneously offer low static contact angle q and low sliding angle u (i.e., minimum tilt angle for a droplet to slide on a surface) for aqueous liquids. Low contact angle q promotes high nucleation rates and low conduction resistance, both of which enhance condensation heat transfer.[31,40,41] Low sliding angle u (due to low contact angle hysteresis Dq) promotes rapid and efficient removal of the condensate droplets, thereby enabling sustained dropwise condensation with significantly higher heat transfer coefficient compared with film-wise condensation.[31,40,41] To demonstrate such enhanced condensation heat transfer, we qualitatively compared the condensation of water (see experimental procedures) on our SLIC surfaces (q z 37, u z 3 for 20 mL water droplets) with condensation on non-slippery hydrophilic surfaces (having low contact angle, but higher sliding angle) and slippery hydrophobic surfaces (having low sliding angle, but higher contact angle). We used untreated silicon

Please cite this article in press as: Vahabi et al., Designing non-textured, all-solid, slippery hydrophilic surfaces, Matter (2022), https://doi.org/10.1016/j.matt.2022.09.024

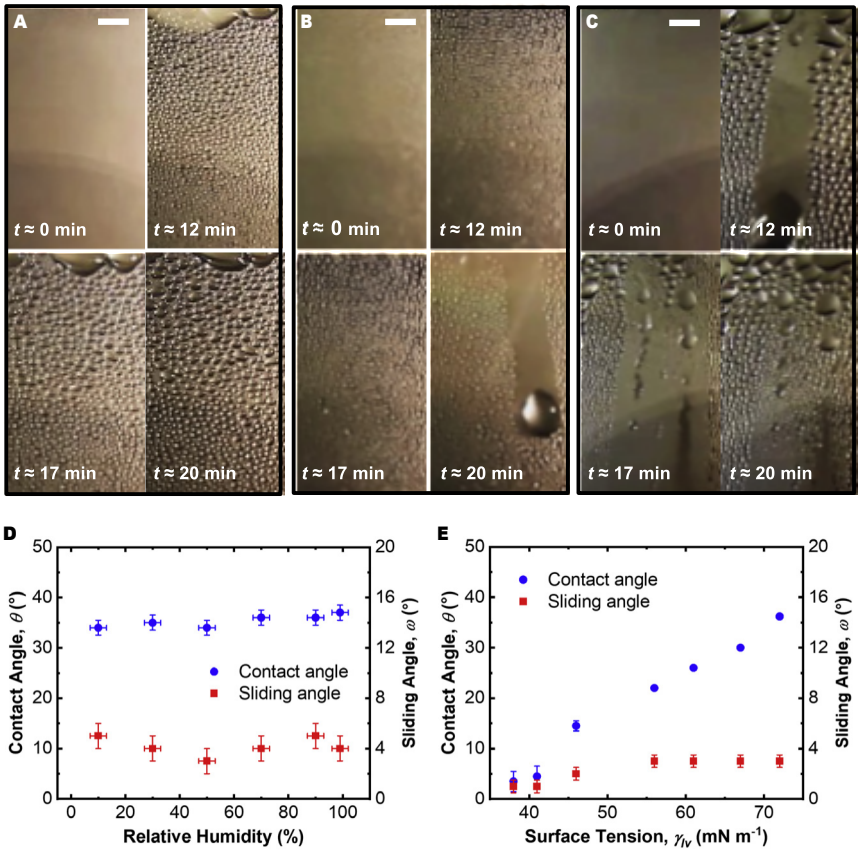

Figure 3. Condensation on SLIC surfaces

(A–C) Water droplet nucleation, growth, and coalescence on vertically oriented non-slippery hydrophilic surface (A), slippery hydrophobic surface (B), and SLIC surface (C), respectively. Upon coalescence, water droplets attained a critical size (z 1.4 mm) and slid down the SLIC surface at a faster rate. Scale bar represents 2 mm for all images.

(D) Static contact angles and sliding angles of water droplets on SLIC surfaces for different relative humidities. Data are represented as mean G standard deviation.

(E) Static contact angles and sliding angles of aqueous liquid droplets with different surface tensions on SLIC surfaces. Data are represented as mean G standard deviation.

wafers as non-slippery hydrophilic surfaces (q z 45, u z 20 for 20 mL water drop-lets) and 1,3-dichlorotetramethyldisiloxane-treated silicon wafers as slippery hydrophobic surfaces (q z 103, q_{adv} z 104, q_{rec} z 101, u z 3 for 20 mL water droplets; see experimental procedures). We exposed vertically mounted surfaces at ambient temperature (z20C) to steam at approximately 100C (see Figures 3A–3C and Video S2). The non-slippery hydrophilic surface and our SLIC surface displayed faster droplet coalescence and growth due to their higher nucleation rate compared with the hydrophobic slippery surface. Condensate droplets attained a critical size (z1.4 mm; see Figure 3C) and slid down our SLIC surface at a faster rate compared with the hydrophobic slippery surface and the non-slippery hydrophilic surface. This rapid droplet shedding indicates that our SLIC surfaces not only facilitate high nucleation rates due to their hydrophilicity but also facilitate rapid condensate removal due to their high slipperiness (i.e., low u). After removal of a condensate droplet, the nucleation, coalescence, growth, and removal of additional condensate droplets continued on our SLIC surface, indicating the potential for sustained dropwise condensation and enhanced condensation heat transfer. In practice, condensation

Please cite this article in press as: Vahabi et al., Designing non-textured, all-solid, slippery hydrophilic surfaces, Matter (2022), https://doi.org/10.1016/j.matt.2022.09.024

can occur at different relative humidities for a wide range of aqueous liquids. To ensure that our SLIC surfaces retain their hydrophilicity and slipperiness, we characterized their contact angles and sliding angles for water at different relative humidities and for aqueous liquids (solutions of sodium dodecyl sulfate in water) with a wide range of surface tensions (g_{lv} = 40 to 72 mN m^{1}; see experimental procedures). Our SLIC surfaces displayed negligible change in static contact angles and sliding angles of water at relative humidities ranging from 10% to 100% (see Figure 3D). As the surface tension of aqueous liquids decreased from 72 to 40 mN m^{1}, our SLIC surfaces displayed an expected decrease in static contact angles and sliding angles (see Figure 3E, Note S3 and Table S3). These results demonstrate the retention of hydrophilicity and slipperiness of our SLIC surfaces and their poten-tial for condensation applications. In addition, our SLIC surfaces also demonstrated the retention of hydrophilicity and slipperiness even after exposure to air for 20 days, immersion in water for 20 days, exposure to steam (at 100C and 1 atm) for a cumulative time of 48 h and 100,000 water droplets sliding past the surface (see Note S4).

In addition to thermofluidic applications, we also evaluated the performance of our SLIC surfaces in biofluidic applications. Specifically, our SLIC surfaces are ideal for fouling-resistant lab-on-a-chip miniature platforms because they simultaneously offer hydrophilicity and slipperiness for aqueous liquids. Hydrophilicity imparted by the PEG brushes allows improved resistance to fouling by proteins because of the hydration layer and the steric hindrance.[42–45] To demonstrate the fouling resistance of our SLIC surfaces, we compared them with that of non-slippery hydrophilic surfaces and slippery hydrophobic surfaces. We used untreated glass coverslips as non-slippery hydrophilic surfaces (q z 53, u z 47 for 20 mL water droplets), 1,3-dichlorotetramethyldisiloxane-treated glass coverslips as slippery hydrophobic surfaces (q z 103, u z 4 for 20 mL water droplets), and glass cover-slips with covalently grafted PEG brushes as our SLIC surfaces (q z 37, u z 5 for 20 mL water droplets). We used glass coverslips because they are smooth (allowing low physical inhomogeneity) and transparent (allowing light microscopy). We exposed the surfaces to fibrinogen solution and studied protein adsorption in situ using total internal reflection fluorescence (TIRF) microscopy (see experimental procedures). Fibrinogen adsorbed within 1 min on both the non-slippery hydrophilic surfaces and slippery hydrophobic surfaces (see Figures 4A and 4B, and Video S3). In contrast, our SLIC surfaces displayed exceptional fouling resistance by preventing adsorption of fibrinogen even at 1,800 min (see Figure 4C and Video S3).[46,47] The exceptional fouling resistance is possibly due to an ice-like hydration layer,[37,38,43] but a comprehensive study is needed to develop a mecha-nistic understanding. In addition to the outstanding fouling resistance, the slipper-iness of our SLIC surfaces allows aqueous droplets to slide easily (see Figure 4D), allowing manipulation of aqueous droplets. To demonstrate the utility of slipper-iness in lab-on-a-chip miniature platforms, we fabricated SLIC surfaces patterned with an array of non-slippery domains (see experimental procedures). When an aqueous droplet (e.g., protein solution) slides past such patterned SLIC surfaces, tiny volumes of the droplet are trapped in the non-slippery domains due to higher adhesion (see Figure 4D and Video S4). In this manner, on patterned SLIC sur-faces, biological analytes (e.g., proteins, nucleic acids, cells, microorganisms, etc.) can be trapped in targeted domains while ensuring that the remaining areas are free of fouling (see Figure 4D). Furthermore, while aqueous droplets slide easily, oil droplets adhere to our SLIC surfaces. When a compound droplet, con-sisting of water and oil, is placed on a tilted SLIC surface, water displaces oil and

Please cite this article in press as: Vahabi et al., Designing non-textured, all-solid, slippery hydrophilic surfaces, Matter (2022), https://doi.org/10.1016/j.matt.2022.09.024

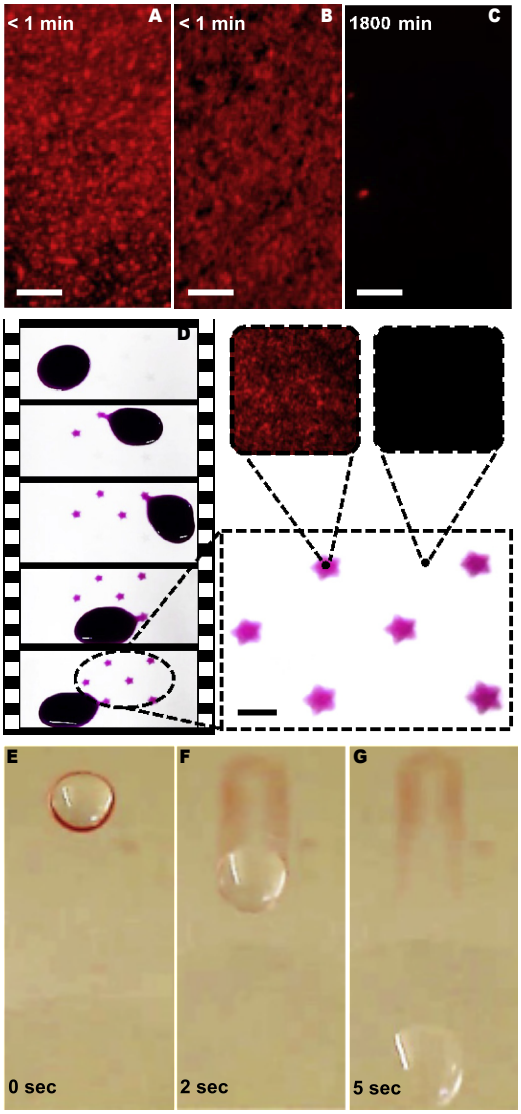

Figure 4. Fouling resistance and oil-water separation on SLIC surfaces

(A) Fluorescent microscopy image showing significant adsorption of fibrinogen (red) on non-slippery hydrophilic surface (surface coverage z 96%) within 1 min. Scale bar represents 5 mm.

(B) Fluorescent microscopy image showing significant adsorption of fibrinogen (red) on slippery hydrophobic surface (surface coverage z 93%) within 1 min. Scale bar represents 5 mm.

(C) Fluorescent microscopy image showing negligible fibrinogen adsorption on SLIC surface (surface coverage z 0.2%), even at 1,800 min. Scale bar represents 5 mm.

(D) Time-lapse images showing tiny volumes of water (pink) trapped in non-slippery domains (star-shaped) when a water droplet slid past a patterned SLIC surface. Inset images showing fibrinogen trapped in the star-shaped domains on the SLIC surface. Scale bar represents 1 mm.

(E) Image showing a compound droplet of water (colorless) and hexadecane (red) on a SLIC surface.

(F) Image showing separation of water (colorless) from hexadecane (red) on the SLIC surface at 2 sec.

(G) Image showing separation of water (colorless) from hexadecane (red) on the SLIC surface at 5 sec.

slides away, while the oil remains adhered (see Figures 4E–4G, Video S5, and Note S5), indicating the potential for biofluidic separations.

Conclusions

In this work, we elucidated the design of non-textured, all-solid, slippery hydrophilic surfaces. We demonstrated two distinct regimes of slipperiness: s < 1, where slipperiness increases with increasing grafting density, and s R 1, where slipperiness is maximum and constant. We postulate that s > 1 is a prudent criterion for the design of non-textured, all-solid, slippery hydrophilic surfaces. Building on this design criterion, we fabricated SLIC surfaces by covalently grafting PEG brushes to silicon wafers and glass coverslips. We demonstrated the exceptional performance of our SLIC surfaces in condensation and fouling resistance compared with non-slippery hydrophilic and slippery hydrophobic surfaces. While a comprehensive study (on processing-structure relationships with a wide variety of chemistries and substrates and the role of ice-like hydration layers) is needed to develop a thorough understanding of this emerging class of surfaces, our results indicate that SLIC surfaces

Please cite this article in press as: Vahabi et al., Designing non-textured, all-solid, slippery hydrophilic surfaces, Matter (2022), https://doi.org/10.1016/j.matt.2022.09.024

have the potential to positively transform the technological landscape of thermofluidic and biofluidic devices.

EXPERIMENTAL PROCEDURES

Resource availability

Lead contact

Further information and requests for resources and materials should be directed to and will be fulfilled by the lead contact, Arun K. Kota (akota2@ncsu.edu).

Materials availability

This study did not generate new unique reagents.

Data and code availability

The data generated during this study are available within the article and its supplemental information files and also are available from the corresponding authors upon reasonable request.

Fabrication of hydrophilic and hydrophobic surfaces

Silicon wafers (<100> orientation; University Wafers) and glass cover slips (Fisher) were cleaned by rinsing thoroughly with acetone (Fisher) and DI water and then dried with nitrogen. The cleaned substrates were exposed to oxygen plasma (Plasma Etch PE-25) for 10 min for hydroxylation. To prepare hydrophilic surfaces, the hydroxylated samples were immersed in a solution consisting of 2 mL of 2-methoxy polyethyleneoxy (6–9) propyl trimethoxysilane (Gelest) and 12 mL hydrochloric acid (Fisher) in 45 mL of anhydrous toluene (Fisher) for the desired time at room temperature. We chose low-molecular-weight PEG silane to reduce steric hindrance and obtain higher grafting densities. To prepare hydrophobic surfaces, the hydroxylated samples were exposed to the vapors of 150 mL of 1,3-dichlorotetramethyldisiloxane (Gelest) in an enclosed chamber for 15 min at room temperature. Finally, the silanized samples were cleaned by rinsing thoroughly with anhydrous toluene, DI water, and ethanol (Fisher) sequentially and then drying with nitrogen.

Fabrication of SLIC surfaces with non-slippery domains

Star-shaped non-slippery domains were fabricated on SLIC surfaces via laser ablation with a commercially available, quasi-continuous CO_2 laser system with a central wavelength of 10.6 mm (Epilog Legend 36EXT). Laser ablation increased the roughness (i.e., physical inhomogeneity), resulting in loss of slipperiness in the domains.

Atomic force microscopy (AFM)

Surface roughness on SLIC surfaces was characterized using AFM (Bruker MultiMode 8-HR) with silicon nitride probes in the ScanAsyst mode. At least 30 images were acquired by scanning 4 3 4 mm areas at a scan rate of 1 Hz and analyzed with Nanoscope Analysis software 1.8 to obtain the root mean square roughness R_{rms}.

X-ray photoelectron spectroscopy (XPS)

The surface chemistry on SLIC surfaces was characterized using XPS (Physical Electronics PHI-5800 spectrometer). XPS was conducted using a monochromatic Al Ka X-ray source operated at 15 kV, and photoelectrons were collected at a takeoff angle of 45 relative to the sample surface. XPS data were acquired from at least five spatially different locations on the surface, and the spectral analysis was conducted using PHI Multipak software.

Please cite this article in press as: Vahabi et al., Designing non-textured, all-solid, slippery hydrophilic surfaces, Matter (2022), https://doi.org/10.1016/j.matt.2022.09.024

Ellipsometry

Ellipsometry was conducted to measure the thickness of PEG layer on SLIC surfaces at different t_{sil} using a variable angle spectroscopic ellipsometer (VASE-VB-250). A spectral scan of the surface was collected between 500 and 900 nm for an incident angle between 55 and 75 with an increment of 5. The thickness of PEG layer (refractive index = 1.45) was determined using a three-layer planar model (air/PEG/silica) of the solid surface from the collected spectra. At least five measurements were conducted at different locations on each surface.

Contact angle, sliding angle, and surface tension measurements

Contact angles and sliding angles were measured with 20 mL sessile droplets, and surface tension was measured with pendant droplets, using a contact angle goniometer/tensiometer (Rame-Hart 260). A custom-built humidity chamber was used to control the humidity. At least six measurements were performed on each surface at spatially distinct locations. The standard deviation is reported as error with all measurements.

Condensation

Water condensation experiments were conducted in a custom-built insulated enclosed chamber equipped with an inlet for steam and a transparent glass window. Steam (at 100C and 1 atm) was generated by boiling water in a conical flask and was directed to the inlet of enclosed chamber through insulated pipes for conden-sation. The substrate was vertically mounted on a Peltier plate set to ambient tem-perature (z 20C), opposite to the glass window, and it was exposed to steam inside the enclosed chamber. The condensation process was monitored and recorded through the glass window using a camera.

Total internal reflection fluorescence microscopy

TIRF microscopy was conducted to study protein adsorption using time-lapse imaging with fibrinogen from human plasma conjugated to Alexa Fluor 647 (Fisher). The time-lapse imaging was conducted using a custom-built microscope[48] equipped with Olympus IX71 body, 100x objective, and a CRISP ASI autofocus system. The excitation was conducted using a 638-nm laser (DL638-328 050, CrystaLaser, Reno, NV). Emission was collected using the appropriate Semrock bandpass filters, and the images were acquired in a water-cooled, back-illuminated EMCCD camera (iXon DU-888, Andor, Belfast, UK) liquid-cooled to 70C with an electronic gain of 60. An enzymatic oxygen scavenging system was used in the imaging buffer to reduce photobleaching.[49] Imaging buffer consisted of 50 mM Tris-HCl (pH 8.0), 10 mM NaCl, 0.15 mg mL^{1} glucose oxidase, 34 mg mL^{1} catalase, 0.8% (w/v) glucose, and 1% (v/v) b-mercaptoethanol. On SLIC surfaces, time-lapse imaging was conducted at a frame rate of 30 frames hr^{1}. On other surfaces, the time-lapse imaging was conducted at a frame rate of 10 frames s^{1}. During imaging, the con-centration of fibrinogen was maintained at 5 nM for all experiments.

SUPPLEMENTAL INFORMATION

Supplemental information can be found online at https://doi.org/10.1016/j.matt.2022.09.024.

ACKNOWLEDGMENTS

We thank Prof. Jan Genzer for insightful discussions and Prof. Brendan O'Connor and Mr. Harry Schrickx for assistance with ellipsometry. A.K.K. gratefully

acknowledges financial support under award 1751628 from the National Science Foundation and under award R01HL135505 from the National Institutes of Health.

AUTHOR CONTRIBUTIONS

A.K.K. conceived the idea. H.V., S.V., M.H., and W.W. conducted experiments. H.V., S.V., D.K., M.J.K., N.M., and A.K.K. conducted the analysis. H.V., S.V., M.H., W.W., D.K., M.J.K., N.M., and A.K.K. wrote the manuscript.

DECLARATION OF INTERESTS

A.K.K. and H.V. are inventors on a patent filed by Colorado State University.

Received: April 18, 2022
Revised: July 19, 2022
Accepted: September 19, 2022
Published: October 7, 2022

REFERENCES

1. Movafaghi, S., Wang, W., Bark, D.L., Dasi, L.P., Popat, K.C., and Kota, A.K. (2019). Hemocompatibility of super-repellent surfaces: current and future. Mater. Horiz. 6, 1596–1610. https://doi.org/10.1039/C9MH00051H.

2. Zhang, P., and Lv, F. (2015). A review of the recent advances in superhydrophobic surfaces and the emerging energy-related applications. Energy 82, 1068–1087. https://doi.org/10.1016/j.energy.2015.01.061.

3. Li, J., Ueda, E., Paulssen, D., and Levkin, P.A. (2019). Slippery lubricant-infused surfaces: properties and emerging applications. Adv. Funct. Mater. 29, 1802317. https://doi.org/10.1002/adfm.201802317.

4. Chen, Y., Lu, K.J., and Chung, T.-S. (2020). An omniphobic slippery membrane with simultaneous anti-wetting and anti-scaling properties for robust membrane distillation. J. Membr. Sci. 595, 117572. https://doi.org/10.1016/j.memsci.2019.117572.

5. Lu, K.J., Zhao, D., Chen, Y., Chang, J., and Chung, T.-S. (2020). Rheologically controlled design of nature-inspired superhydrophobic and self-cleaning membranes for clean water production. npj Clean Water 3, 1–10. https://doi.org/10.1038/s41545-020-0078-2.

6. Lu, K.-J., Liang, C.Z., Chen, Y., and Chung, T.-S. (2022). Unlock the secret of air blowing in developing high strength and superhydrophobic membranes for membrane distillation. Desalination 527, 115579. https://doi.org/10.1016/j.desal.2022.115579.

7. Hamrock, B.J., Schmid, S.R., and Jacobson, B.O. (2004). Fundamentals of Fluid Film Lubrication (CRC press).

8. Movafaghi, S., Cackovic, M.D., Wang, W., Vahabi, H., Pendurthi, A., Henry, C.S., and Kota, A.K. (2019). Superomniphobic papers for on-paper pH sensors. Adv. Mater. Interfac. 6, 1900232. https://doi.org/10.1002/admi.201900232.

9. Vallabhuneni, S., Movafaghi, S., Wang, W., and Kota, A.K. (2018). Superhydrophobic coatings for improved performance of electrical insulators. Macromol. Mater. Eng. 303, 1800313. https://doi.org/10.1002/mame.201800313.

10. Tuteja, A., Choi, W., Ma, M., Mabry, J.M., Mazzella, S.A., Rutledge, G.C., McKinley, G.H., and Cohen, R.E. (2007). Designing superoleophobic surfaces. Science 318, 1618–1622. https://doi.org/10.1126/science.1148326.

11. Wang, W., Vahabi, H., Movafaghi, S., and Kota, A.K. (2019). Superomniphobic surfaces with improved mechanical durability: synergy of hierarchical texture and mechanical interlocking. Adv. Mater. Interfac. 6, 1900538. https://doi.org/10.1002/admi.201900538.

12. Vahabi, H., Wang, W., Popat, K.C., Kwon, G., Holland, T.B., and Kota, A.K. (2017). Metallic superhydrophobic surfaces via thermal sensitization. Appl. Phys. Lett. 110, 251602. https://doi.org/10.1063/1.4989577.

13. Lee, C., Choi, C.-H., and Kim, C.-J. (2016). Superhydrophobic drag reduction in laminar flows: a critical review. Exp. Fluid 57, 176–220. https://doi.org/10.1007/s00348-016-2264-z.

14. Rothstein, J.P. (2010). Slip on superhydrophobic surfaces. Annu. Rev. Fluid Mech. 42, 89–109. https://doi.org/10.1146/annurev-fluid-121108-145558.

15. Epstein, A.K., Wong, T.-S., Belisle, R.A., Boggs, E.M., and Aizenberg, J. (2012). Liquid-infused structured surfaces with exceptional anti-biofouling performance. Proc. Natl. Acad. Sci. USA 109, 13182–13187. https://doi.org/10.1073/pnas.1201973109.

16. Irajizad, P., Hasnain, M., Farokhnia, N., Sajadi, S.M., and Ghasemi, H. (2016). Magnetic slippery extreme icephobic surfaces. Nat. Commun. 7, 13395–13397. https://doi.org/10.1038/ncomms13395.

17. Solomon, B.R., Khalil, K.S., and Varanasi, K.K. (2014). Drag reduction using lubricant-impregnated surfaces in viscous laminar flow. Langmuir 30, 10970–10976. https://doi.org/10.1021/la5021143.

18. Tian, X., Verho, T., and Ras, R.H.A. (2016). Moving superhydrophobic surfaces toward real-world applications. Science 352, 142–143. https://doi.org/10.1126/science.aaf2073.

19. Peppou-Chapman, S., Hong, J.K., Waterhouse, A., and Neto, C. (2020). Life and death of liquid-infused surfaces: a review on the choice, analysis and fate of the infused liquid layer. Chem. Soc. Rev. 49, 3688–3715. https://doi.org/10.1039/D0CS00036A.

20. Hoque, M.J., Sett, S., Yan, X., Liu, D., Rabbi, K.F., Qiu, H., Qureshi, M., Barac, G., Bolton, L., and Miljkovic, N. (2022). Life span of slippery lubricant infused surfaces. ACS Appl. Mater. Interfaces 14, 4598–4611. https://doi.org/10.1021/acsami.1c17010.

21. Sett, S., Oh, J., Cha, H., Veriotti, T., Bruno, A., Yan, X., Barac, G., Bolton, L.W., and Miljkovic, N. (2021). Lubricant-infused surfaces for low-surface-tension fluids: the extent of lubricant miscibility. ACS Appl. Mater. Interfaces 13, 23121–23133. https://doi.org/10.1021/acsami.1c02716.

22. Ma, J., Sett, S., Cha, H., Yan, X., and Miljkovic, N. (2020). Recent developments, challenges, and pathways to stable dropwise condensation: a perspective. Appl. Phys. Lett. 116, 260501. https://doi.org/10.1063/5.0011642.

23. Buddingh, J.V., Hozumi, A., and Liu, G. (2021). Liquid and liquid-like surfaces/coatings that readily slide fluids. Prog. Polym. Sci. 123, 101468. https://doi.org/10.1016/j.progpolymsci.2021.101468.

24. Wang, L., and McCarthy, T.J. (2016). Covalently attached liquids: instant omniphobic surfaces with unprecedented repellency. Angew Chem. Int. Ed. Engl. 55, 244–248. https://doi.org/10.1002/anie.201509385.

25. Wang, X., Wang, Z., Heng, L., and Jiang, L. (2020). Stable omniphobic anisotropic covalently grafted slippery surfaces for directional transportation of drops and bubbles. Adv. Funct. Mater. 30, 1902686. https://doi.org/10.1002/adfm.201902686.

26. Zhao, H., Deshpande, C.A., Li, L., Yan, X., Hoque, M.J., Kuntumalla, G., Rajagopal, M.C., Chang, H.C., Meng, Y., Sundar, S., et al. (2020). Extreme antiscaling performance of slippery omniphobic covalently attached liquids. ACS Appl. Mater. Interfaces 12, 12054–12067. https://doi.org/10.1021/acsami.9b22145.

27. Zhao, H., Khodakarami, S., Deshpande, C.A., Ma, J., Wu, Q., Sett, S., and Miljkovic, N. (2021). Scalable slippery omniphobic covalently attached liquid coatings for flow fouling reduction. ACS Appl. Mater. Interfaces 13, 38666–38679. https://doi.org/10.1021/acsami.1c08845.

28. Nakamura, S., Archer, R.J., Dunderdale, G.J., and Hozumi, A. (2020). Perfluorinated compounds are not necessary: pegylated organosilanes can endow good water sliding/removal properties. J. Hazard Mater. 398, 122625. https://doi.org/10.1016/j.jhazmat.2020.122625.

29. Becher-Nienhaus, B., Liu, G., Archer, R.J., and Hozumi, A. (2020). Surprising lack of influence on water droplet motion by hydrophilic microdomains on checkerboard-like surfaces with matched contact angle hysteresis. Langmuir 36, 7835–7843. https://doi.org/10.1021/acs.langmuir.0c00808.

30. Papra, A., Gadegaard, N., and Larsen, N.B. (2001). Characterization of ultrathin poly (ethylene glycol) monolayers on silicon substrates. Langmuir 17, 1457–1460. https://doi.org/10.1021/la000609d.

31. Cha, H., Vahabi, H., Wu, A., Chavan, S., Kim, M.K., Sett, S., Bosch, S.A., Wang, W., Kota, A.K., and Miljkovic, N. (2020). Dropwise condensation on solid hydrophilic surfaces. Sci. Adv. 6, eaax0746. https://doi.org/10.1126/sciadv.aax0746.

32. Rubinstein, M., and Colby, R.H. (2003). Polymer Physics, 23 (Oxford university press).

33. Ulman, A. (1996). Formation and structure of self-assembled monolayers. Chem. Rev. 96, 1533–1554. https://doi.org/10.1021/cr9502357.

34. Johnson, R.E., Jr., and Dettre, R.H. (1964). Contact angle hysteresis: I. Study of an idealized rough surface. ACS Adv. Chem. Ser. 43, 112–135. https://doi.org/10.1021/ba-1964-0043.ch007.

35. Dettre, R.H., and Johnson, R.E., Jr. (1964). Contact angle hysteresis: II. Contact angle measurements on rough surfaces. ACS Adv. Chem. Ser. 43, 136–144. https://doi.org/10.1021/ba-1964-0043.ch008.

36. Ho, T.A., Papavassiliou, D.V., Lee, L.L., and Striolo, A. (2011). Liquid water can slip on a hydrophilic surface. Proc. Natl. Acad. Sci. USA 108, 16170–16175. https://doi.org/10.1073/pnas.1105189108.

37. Ma, L., Gaisinskaya-Kipnis, A., Kampf, N., and Klein, J. (2015). Origins of hydration lubrication. Nat. Commun. 6, 6060–6066. https://doi.org/10.1038/ncomms7060.

38. Pertsin, A.J., and Grunze, M. (2000). Computer simulation of water near the surface of oligo (ethylene glycol)-terminated alkanethiol self-assembled monolayers. Langmuir 16, 8829–8841. https://doi.org/10.1021/la000340y.

39. Brzoska, J.B., Azouz, I.B., and Rondelez, F. (1994). Silanization of solid substrates: a step toward reproducibility. Langmuir 10, 4367–4373. https://doi.org/10.1021/la00023a072.

40. El Fil, B., Kini, G., and Garimella, S. (2020). A review of dropwise condensation: theory, modeling, experiments, and applications. Int. J. Heat Mass Tran. 160, 120172. https://doi.org/10.1016/j.ijheatmasstransfer.2020.120172.

41. Ho, J.Y., Rabbi, K.F., Khodakarami, S., Ma, J., Boyina, K.S., and Miljkovic, N. (2022). Opportunities in nanoengineered surface designs for enhanced condensation heat and mass transfer. J. Heat Tran. 144, 050801. https://doi.org/10.1115/1.4053454.

42. Jeon, S., Lee, J., Andrade, J., and De Gennes, P. (1991). Protein—surface interactions in the presence of polyethylene oxide: I. Simplified theory. J. Colloid Interface Sci. 142, 149–158. https://doi.org/10.1016/0021-9797(91)90043-8.

43. Sayin, M., Nefedov, A., and Zharnikov, M. (2020). Interaction of water with oligo (ethylene glycol) terminated monolayers: wetting versus hydration. Phys. Chem. Chem. Phys. 22, 8088–8095. https://doi.org/10.1039/D0CP00906G.

44. Hedayati, M., Krapf, D., and Kipper, M.J. (2021). Dynamics of long-term protein aggregation on low-fouling surfaces. J. Colloid Interface Sci. 589, 356–366. https://doi.org/10.1016/j.jcis.2021.01.001.

45. Hedayati, M., Kipper, M.J., and Krapf, D. (2020). Anomalous protein kinetics on low-fouling surfaces. Phys. Chem. Chem. Phys. 22, 5264–5271. https://doi.org/10.1039/D0CP00326C.

46. Worz, A., Berchtold, B., Moosmann, K., Prucker, O., and Ruhe, J. (2012). Protein-resistant polymer surfaces. J. Mater. Chem. 22, 19547–19561. https://doi.org/10.1039/C2JM30820G.

47. Chen, S., Li, L., Zhao, C., and Zheng, J. (2010). Surface hydration: principles and applications toward low-fouling/nonfouling biomaterials. Polymer 51, 5283–5293. https://doi.org/10.1016/j.polymer.2010.08.022.

48. Weigel, A.V., Simon, B., Tamkun, M.M., and Krapf, D. (2011). Ergodic and nonergodic processes coexist in the plasma membrane as observed by single-molecule tracking. Proc. Natl. Acad. Sci. USA 108, 6438–6443. https://doi.org/10.1073/pnas.1016325108.

49. Hedayati, M., Marruecos, D.F., Krapf, D., Kaar, J.L., and Kipper, M.J. (2020). Protein adsorption measurements on low fouling and ultralow fouling surfaces: a critical comparison of surface characterization techniques. Acta Biomater. 102, 169–180. https://doi.org/10.1016/j.actbio.2019.11.019.

Matter, Volume 5

Supplemental information

Designing non-textured, all-solid,

slippery hydrophilic surfaces

Hamed Vahabi, Sravanthi Vallabhuneni, Mohammadhasan Hedayati, Wei Wang, Diego Krapf, Matt J. Kipper, Nenad Miljkovic, and Arun K. Kota

Supplemental Notes and Supplemental Experimental Procedures.

Note S1. Estimation of non-dimensional slipperiness factor σ^*

The non-dimensional slipperiness factor σ^* at different silanization times $t_{silanization}$ is defined as $\sigma^* = \sigma/\sigma_{crit}$. Grafting density σ (in chains nm^{-2}) on SLIC surfaces was estimated using $\sigma = (h\rho N_A \times 10^{-21})/M$;[1] here, h is the thickness of the PEG layer (in nm) estimated using ellipsometry (see Experimental Procedures), ρ = 1.075 g cm^{-3} is the density of PEG, N_A = 6.023 x 10^{23} is Avogadro's number, and M = 330 Da is the average molecular weight of PEG with 6 to 9 monomers. In order to estimate the critical grafting density σ_{crit} (i.e., the grafting density σ when the tethered brush size is equal to the inter-tether distance), we chose hexagonal packing of PEG brushes (because it is a preferred geometry in nature, and it provides a constant inter-brush spacing making the analysis simpler). With a hexagonal packing of PEG brushes (see Figure S1), we estimated the critical grafting density using Eq. S1.

$$\sigma_{crit} = \frac{Chains\ per\ unit\ cell}{Area\ of\ unit\ cell} = \frac{3}{(6\sqrt{3}R_g^2)} = \frac{1}{2\sqrt{3}R_g^2} \qquad \text{(S1)}$$

The average Flory radius[2] $R_g = lN^{0.6} \approx 0.58$ nm for PEG brushes with monomer length[3], l = 0.3 nm and number of monomers, N = 6 to 9. The non-dimensional slipperiness factor σ^* at different silanization times $t_{silanization}$ are reported in Table S1.

Note S2. Designing SLIC surfaces with $PEG_{9\text{-}12}$

To validate our design criteria for SLIC surfaces, we designed SLIC surfaces using PEG brushes with 9-12 repeating units ($PEG_{9\text{-}12}$, average molecular weight $M \approx 462$ Da), in addition to PEG brushes with 6-9 repeating units ($PEG_{6\text{-}9}$, average molecular weight $M \approx 330$ Da). We fabricated SLIC surfaces by covalently grafting $PEG_{9\text{-}12}$ brushes to hydroxylated smooth silicon wafers using liquid phase silanization (see experimental procedures). We systematically tuned the non-dimensional slipperiness factor σ^* by tailoring the silanization time $t_{silanization}$ (see Table S2). At different $t_{silanization}$, we estimated σ using the PEG layer thickness h obtained from ellipsometry (see main manuscript and experimental procedures). Assuming hexagonal packing, we estimated σ_{max} for $PEG_{9\text{-}12}$ (see Note S1). As anticipated, at $t_{silanization}$ = 0 min, water droplets completely spread and did not slide on hydroxylated silicon wafers. As $t_{silanization}$ increased, the dynamic contact angles (θ_{adv} and θ_{rec}) of water increased (see Figure S2A), indicating increasing covalent grafting of $PEG_{9\text{-}12}$ brushes, resulting in increasing σ^*. Simultaneously, as $t_{silanization}$ increased, $\Delta\theta$ decreased (see Figure S2B), indicating a decrease in inhomogeneities on the surface as $\sigma^* \rightarrow 1$. At $t_{silanization}$ = 7 min, we estimated $\sigma^* > 1$ for $PEG_{9\text{-}12}$ brushes, indicating the onset of maximum and constant slipperiness regime with $\theta_{adv} = 39°$, $\theta_{rec} = 36°$, and $\Delta\theta = 3°$. For $t_{silanization} > 7$ min, we obtained SLIC surfaces with nearly constant contact angles and contact angle hysteresis (see Figures S2A and S2B). Here, it is noteworthy that while the onset of slipperiness did not change between $PEG_{9\text{-}12}$ and $PEG_{6\text{-}9}$, σ^* and σ for $PEG_{9\text{-}12}$ and $PEG_{6\text{-}9}$ are different (see Table S1 and Table S2). This further reaffirms our design criteria for SLIC surfaces ($\sigma^* > 1$).

Note S3. Estimation of sliding angles

The sliding angles ω were estimated based on a balance between work done by gravitational force and work expended due to adhesion as:[4]

$$\sin\omega \approx \frac{\gamma_{\$1} D_{345}(\cos\theta_{\&2\%} - \cos\theta_{/01})}{\rho g V} \tag{S2}$$

Here, $\gamma_{\$1}$, ρ and V are surface tension, density, and volume of the liquid droplet, respectively, g is the acceleration due to gravity, $\theta_{/01}$ and $\theta_{\&2\%}$ are the advancing and receding contact angles, respectively, and D_{345} is the width of the triple phase contact line perpendicular to the droplet sliding direction. Assuming the droplet is a spherical cap, width of the triple phase contact line was calculated as:

$$D_{345} = 2\sin\theta \left(\frac{3V}{\pi(2 - 3\cos\theta + \cos^{-}\theta)}\right)^{\frac{+}{-}} \tag{S3}$$

Here, θ is the average contact angle, given as:

$$\cos\theta = \frac{(\cos\theta_{/01} + \cos\theta_{\&2\%})}{2} \tag{S4}$$

The estimated sliding angles for 20 ∝L droplets of SDS in water solutions on SLIC surfaces were obtained using Eq. S2-S4 and reported in Table S3.

Note S4. Durability of SLIC surfaces

We investigated the durability (i.e., retention of hydrophilicity and slipperiness) of our SLIC surfaces after prolonged exposure to air, immersion in water, exposure to steam (at 100°C and 1 atm), and water droplets (30 ∝L) sliding past the surface. We measured the advancing and receding contact angles as well as the sliding angles periodically to assess the hydrophilicity and slipperiness. Our results indicated no change in advancing and receding contact angles and sliding angles on SLIC surfaces even after exposure to air for 20 days (see Figure S3A), immersion in water for 20 days (see Figure S3B), exposure to steam for a cumulative time of 48 hours (see Figure S3C) with dropwise condensation and 100,000 water droplets sliding past the surface (see Figure S3D). While these results demonstrate the potential of SLIC surfaces, a more comprehensive and application-specific determination of durability is needed for lasting use in themofluidic and biofluidic applications.

Note S5. Energy analysis for a compound droplet of water and oil

For our SLIC surfaces, we determined the surface energy $\gamma_{s1} = \gamma_{s1}^{6} + \gamma_{s1}^{0}$ = 22 mN m^{-1} + 44 mN m^{-1} = 66 mN m^{-1} using the Owens-Wendt analysis[5], with water (polar liquid) and methylene iodide (non-polar liquid) as probe liquids. To separate a compound droplet of water and oil using our SLIC surfaces, water must displace oil from the SLIC surface so that it can slide away while leaving the oil adhered. To determine whether or not water displaces oil from the SLIC surface, we compared the energy of two configurations (see Figures S4A and S4B) – oil displacing water on a SLIC surface (with energy $E_1 = \gamma_{s7} + \gamma_{78} + \gamma_{81}$) and water displacing oil on a SLIC surface (with energy $E_2 = \gamma_{s8} + \gamma_{78} + \gamma_{71}$). Here, water surface tension $\gamma_{81} = \gamma_{81}^{6} + \gamma_{81}^{0}$ = 51 mN m^{-1} + 21 mN m^{-1} = 72 mN m^{-1} and hexadecane (oil) surface tension $\gamma_{71} = \gamma_{71}^{0}$ = 27.5 mN m^{-1}. As postulated by Fowkes[6], we estimated $\gamma_{s7} = \gamma_{s1} + \gamma_{71} - 2Z\sqrt{\gamma_{s1}^{0}\,\gamma_{71}^{0}}$ = 24 mN m^{-1} and $\gamma_{78} = \gamma_{71} + \gamma_{81} - 2Z\sqrt{\gamma_{71}^{0}\,\gamma_{81}^{0}}$ = 51 mN m^{-1}. As postulated by Owens and Wendt[5], we estimated $\gamma_{s8} = \gamma_{s1} + \gamma_{81} - 2Z\sqrt{\gamma_{s1}^{0}\,\gamma_{81}^{0}} - 2\,[\sqrt{\gamma_{s1}^{6}\,\gamma_{81}^{6}}$ = 10 mN m^{-1}. This energy analysis shows E_2 = 89 mN m^{-1} < E_1 = 133 mN m^{-1}, indicating water indeed displaces oil from SLIC surfaces (see Figures S4C-E).

Supplemental Figures and Tables

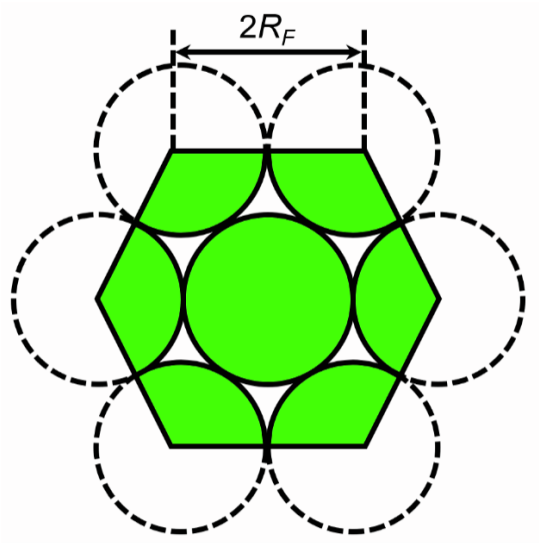

Figure. S1. Schematic depicting the hexagonal packing of PEG brushes (green) at critical grafting density $\sigma_{\%\&\#}$. Schematic not to scale.

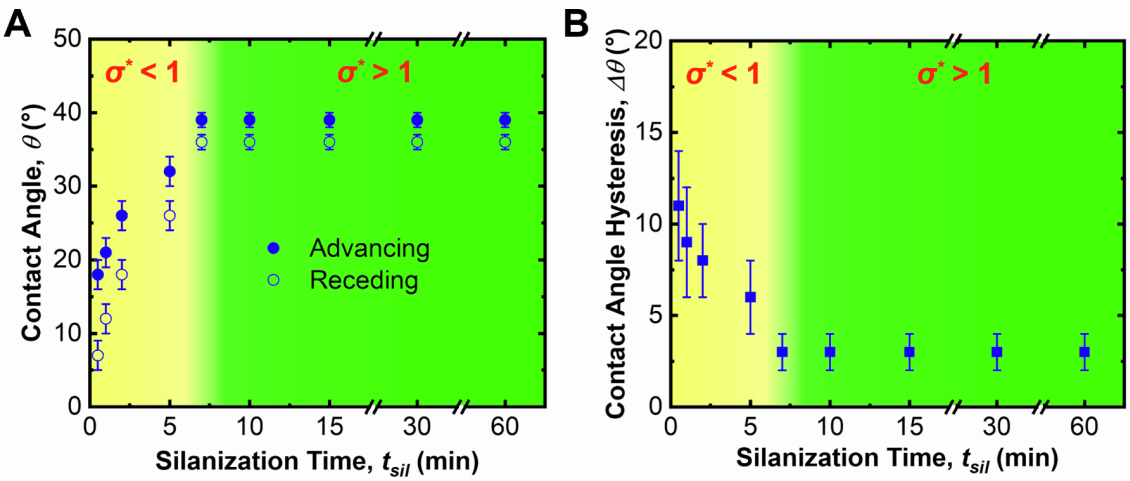

Figure. S2. Contact angles and contact angle hysteresis of water on $PEG_{9\text{-}12}$ functionalized surfaces. (A) and (B) Advancing and receding contact angles, and contact angle hysteresis, respectively, of water on $PEG_{9\text{-}12}$ functionalized surfaces at different silanization times, $t_{"\#\$}$.

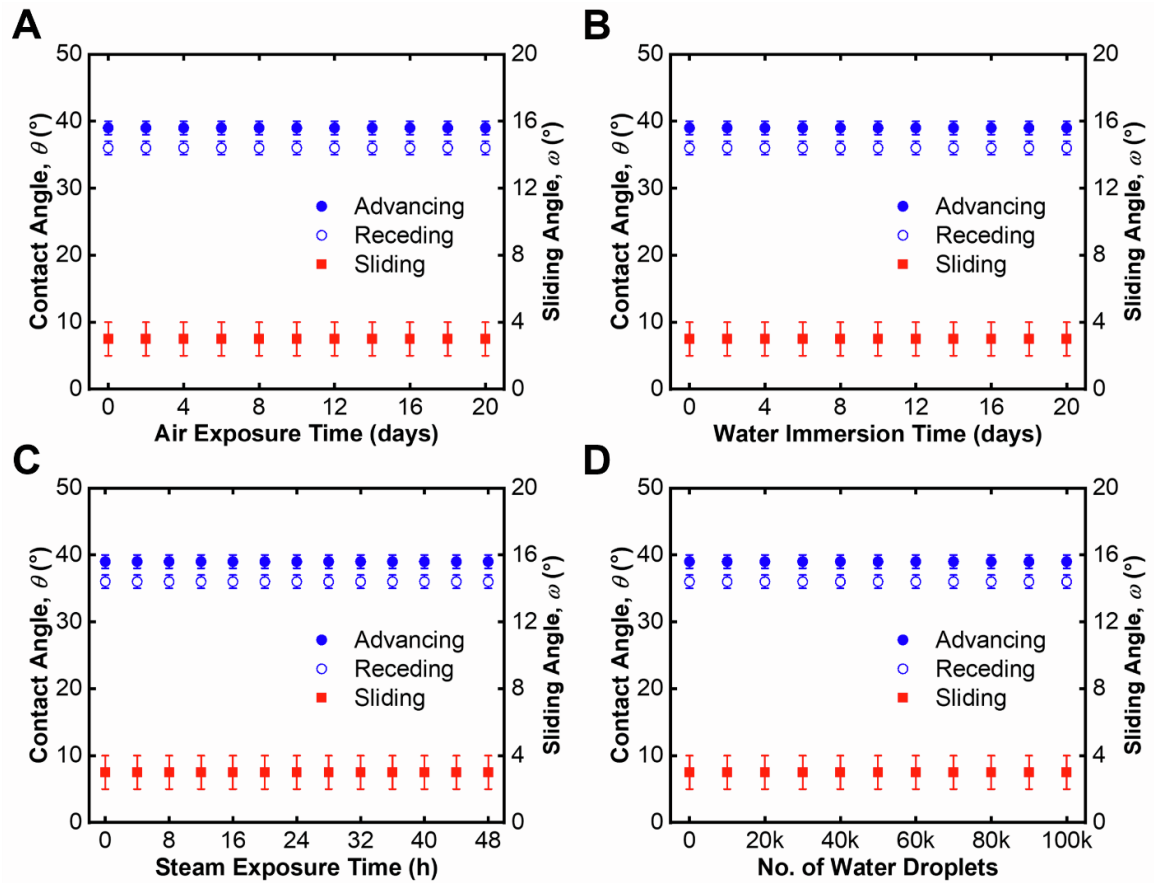

Figure. S3. Durability of SLIC surfaces. (A), (B), (C) and (D) Advancing and receding contact angles and sliding angles of water on a SLIC surface as a function of air exposure time, water immersion time, steam exposure time and number of water droplets sliding past the surface, respectively.

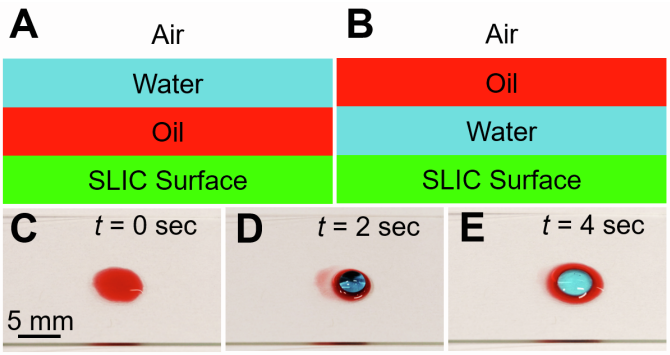

Figure. S4. Configurations of oil and water on SLIC surfaces. (A) and (B) Schematics showing configurations of our SLIC surface with oil displacing water and water displacing oil, respectively. Schematics not to scale. (C). Hexadecane droplet (red) on a SLIC surface. (D) Water droplet (blue) placed on top of the hexadecane droplet on the SLIC surface. (E) Within a few seconds, water displaced hexadecane from the SLIC surface.

Table S1. Non-dimensional slipperiness factor σ^* with PEG (6-9 repeating units) at different silanization times $t_{"\#\$}$.

$t_{"\#\$}$ (min)	h (nm)	σ (chains nm^{-2})	σ^*
0.5	0.15 ± 0.03	0.29	0.34
1	0.19 ± 0.01	0.38	0.44
2	0.33 ± 0.13	0.65	0.77
5	0.43 ± 0.01	0.84	0.99
7	0.59 ± 0.21	1.16	1.37
10	0.65 ± 0.05	1.28	1.51
15	0.84 ± 0.15	1.65	1.95
30	0.93 ± 0.06	1.82	2.15
60	1.01 ± 0.06	1.98	2.34

Table S2. Non-dimensional slipperiness factor σ^* with PEG (9-12 repeating units) at different silanization times $t_{"\#\$}$.

$t_{"\#\$}$ (min)	h (nm)	σ (chains nm^{-2})	σ^*
0.5	0.15 ± 0.01	0.21	0.31
1	0.17 ± 0.01	0.24	0.35
2	0.25 ± 0.04	0.35	0.52
5	0.38 ± 0.03	0.53	0.79
7	0.52 ± 0.02	0.73	1.08
10	0.76 ± 0.31	1.06	1.58
15	1.09 ± 0.05	1.53	2.27
30	1.34 ± 0.12	1.88	2.79
60	1.62 ± 0.14	2.27	3.37

Table S3. Estimated and measured sliding angles of SDS in water solutions on SLIC surfaces.

$\gamma_{\$1}$ (mN m^{-1})	$\omega_{9:;<=>;9?}$ (°)	$\omega_{=9>:@A9?}$ (°)
72	4.4	3
67	3.6	3
61	3.1	3
56	2.5	3
46	2.2	2
41	1.2	1
38	1.1	1

Supplemental References

1. Luzinov, I., Julthongpiput, D., Malz, H., Pionteck, J. and Tsukruk, V. V. (2000). Polystyrene layers grafted to epoxy-modified silicon surfaces. *Macromolecules 33(3)*, 1043-1048. 10.1021/ma990926v.
2. Rubinstein, M. and Colby, R. H. (2003). Polymer physics. (Oxford university press), vol. 23.
3. Israelachvili, J. N. (2011). Intermolecular and surface forces. (Academic Press).
4. Furmidge, C. G. L. (1962). Studies at phase interfaces. I. The sliding of liquid drops on solid surfaces and a theory for spray retention. *J. Colloid Sci. 17(4)*, 309-324. 10.1016/0095-8522(62)90011-9.
5. Owens, D. K. and Wendt, R. (1969). Estimation of the surface free energy of polymers. *J. Appl. Poly. Sci. 13(8)*, 1741-1747. 10.1002/app.1969.070130815.
6. Fowkes, F. M. (1964). Attractive forces at interfaces. *Ind. Eng. Chem. 56(12)*, 40-52. 10.1021/ie50660a008.